Magmatic intrusion-related processes in the upper lunar crust: The role of country rock porosity/permeability in magmatic percolation and thermal annealing, and implications for gravity signatures.

James W. Head[1] and Lionel Wilson[1,2]

[1]Department of Earth, Environmental and Planetary Sciences, Brown University, Providence, RI 02912 USA

[2]Lancaster Environment Centre, Lancaster University, Lancaster LA1 4YQ UK

Abstract: Shallow crustal country rock on the Moon is demonstrably more fractured and porous than deeper crustal bedrock, and Gravity Recovery and Interior Laboratory (GRAIL) mission gravity data have shown that deeper crustal bedrock is more porous than previously thought. This raises the question of how crustal porosity and permeability will influence the nature of magmatic dike intrusions in terms of: 1) the ability of intruding magma to inject into and occupy this pore space (shallow magmatic percolation), 2) the influence of the intruded magma on annealing of this porosity and permeability (thermal annealing), both 1 and 2 densify the country rock), and 3) the effect of crustal porosity on favoring sill formation as a function of depth in the lunar crust. We analyze quantitatively the emplacement of basaltic dikes and sills on the Moon and assess these three factors in the context of the most recent data on micro- and macro-scale porosity of lunar crustal materials. For the range of plausible micro/macro-scale porosity and permeability determined by crack widths (mm to cm) and open crack lateral continuity (mm to tens of cm), we find that 1) rapid conductive cooling of injected magma due to the very large surface area to volume ratio restricts magmatic percolation to very limited zones (extending for at most several tens of cm) adjacent to the ascending dike or intruded sill, even in the upper several hundred meters of the lunar crust; 2) the conductive heat loss from intruded dikes and sills results in a thermal wave decay rate that is predicted to limit the extent of intrusion-adjacent thermal annealing to less than ~6% of the thickness of the intruded body; 3) the extremely rapid rise rate of magma in dikes originating from sources in the lunar mantle disfavors the lateral migration of dikes to form sills in the crust, except in specific shallow crustal locations influenced by impact crater-related environments (e.g., floor-fractured craters). We conclude that, although magmatic percolation and thermal annealing in association with lunar mare

basalt magmatic dike and sill emplacement should be taken into consideration in interpreting gravity signatures, the effects are likely to be minor compared with the density contrast of the solidified basaltic magmatic intrusion itself.

I. Introduction and Background:

The anorthositic lunar crust is interpreted to have formed by large-scale melting and plagioclase flotation in a magma ocean context in the earliest part of lunar history (see reviews in Shearer et al., 2006; Wieczorek et al., 2006). During and subsequent to its formation the crust has been subjected to 1) thermal stresses associated with both initial magma ocean cooling and solidification, and longer-term global cooling, 2) tectonic flexure, fracturing and deformation associated with loading and thermal evolution, and 3) impact-related fracturing, plastic and viscous deformation and melting at a wide range of scales (micro-craters to basins) (Figure 1a). All of these processes can produce variations in density and porosity at a range of scales and depths in the lunar crust (Figure 1b).

Estimates of the density structure of the lunar crust were made initially from Apollo seismic data (summarized in Lognonné et al., 2003) and showed that the upper crust (the megaregolith and most highly fractured bedrock) extended to ~20 km depth, at which depth seismic velocities were constant with depth until the crust-mantle boundary was reached. The seismic velocity transition at about 20 km depth was interpreted to be the depth at which overburden pressure closed the cracks in the fractured bedrock (Figure 1b).

Subsequently, Kiefer et al. (2012) measured the density and porosity of a suite of lunar rocks (Apollo samples and lunar meteorites) and provided more accurate values for representative lunar crustal materials, including impact basin ejecta. Recently, the Gravity Recovery and Interior Laboratory (GRAIL) mission (Zuber et al., 2013) provided high-resolution gravity data that were used to show that the bulk density of the highlands crust was 2550 kg/m^3 (Wieczorek et al., 2013), substantially lower than the 2800-2900 kg/m^3 previously used in geophysical models of anorthositic crustal materials (Wieczorek at el., 2006). These new data, combined with the Kiefer et al. (2012) updated density and porosity measurements for lunar materials, led to the interpretation that the average crustal porosity is ~12% (ranging from 4-21%) (Wieczorek et al., 2013). Surface and near-surface densities are interpreted to be much lower, about 2223 kg/m^3 and corresponding porosities to be higher, 22-26% (Besserer et al., 2014). This low bulk crustal density, together with the Apollo seismic constraints, led to a crust model that estimated average crustal thickness values between 34 and 43 km (Wieczorek et al., 2013) (Figure 1b).

The low crustal density values were attributed by Wieczorek et al. (2013) and Besserer et al. (2014) to be due to impact-induced fractures and brecciation (Figure 1); lateral variations were correlated with recent impact basin ejecta (lower density, such as ballistic emplacement and substrate shock-wave deformation surrounding the Orientale basin) and basin interiors (higher density, attributed to substantial thermal annealing). Indeed, analysis of GRAIL data for about 1200 complex craters by Soderblom et al. (2015) showed that larger craters produce more extensive fractures and dilatant bulking, leading to an estimate of the thickness of the impact-induced megaregolith of at least 8 km (Figure 1b). Estimating the actual change in density structure with depth is more difficult, however, due in part to the processes operating to close fractures and increase density with depth. In general, there are two candidate processes for pore-closure with depth: 1) Han et al. (2014), using GRAIL data, found the surface density of megaregolith to be about 2400 kg/m3 with an initial porosity of ~10-20%; this porosity was estimated to be eliminated at about 10-20 km depth due to lithostatic overburden pressure (Figure 1b). 2) Wieczorek et al. (2013) called on viscous deformation due to increasing temperatures with depth to decrease porosity and increase density. Because of the strong temperature dependence of viscosity, these changes were interpreted to occur over a narrow depth interval (<5 km). Wieczorek et al. (2013) used representative temperature gradients over lunar history and found that, depending on the heat fluxes and rheologies assumed, the minimum depth at which this transition would take place is ~40 km. On the basis of these considerations, we infer a three-layer crustal configuration as follows (Figure 1b): 1) An upper layer of low-density megaregolith transitioning with depth into first, allocthonous breccias, and then autocthonous (in situ) brecciated bedrock (~10-20 km thick); 2) An intermediate layer below about 10-20 km where overburden pressure has largely closed cracks in the crust (Han et al., 2014); 3) A deeper layer (in excess of 40 km) where thermal annealing (viscous deformation at elevated temperatures) (Wieczorek et al., 2013; Besserer et al., 2014) together with overburden pressure combine to close cracks and pore spaces. We now utilize this crustal framework (Figure 1b) to investigate potential processes related to basaltic magmatic intrusion into the crust (dikes and sills) and their effects on modifying the density structure and gravity signatures of the crust. The effects of gas exsolution and bubble coalescence on shallow sill structure, evolution, density and surface topography in floor-fractured craters have been treated previously by Wilson and Head (2018a) and are not repeated here.

II. Processes Associated with Dike Emplacement and Sill Intrusions into the Lunar Crust:

Magma generated at depth in the lunar interior ascends through the mantle and crust before erupting onto the surface of the Moon. Wilson and Head (1981, 2017a,b, 2018a,b) and Head and Wilson (1992, 2017) have explored the basic principles of the generation, ascent and eruption of basaltic magma on the Moon, assessed the likelihood, characteristics and evolution of shallow sill-like intrusions, and correlated the predictable stages in lunar eruptions with the range of extrusive and intrusive landforms. Untreated in these analyses were the detailed roles of minor intrusions into cracks adjacent to a dike or sill, and the thermal effects on the surrounding country rock in terms of annealing and consequent modification of country rock density and porosity.

In a regional study, Kiefer (2013) analyzed basaltic intrusions interpreted to have been emplaced in the shallow crust in the Marius Hills region of the Moon and assessed their role in changing the density structure of the shallow crust through 1) the addition of the intrusion itself (dikes and sills), 2) the closing of pore space by magmatic infiltration into void space (envisioned as a connected network of cracks and pores; see Kiefer, 2013, his Figure 10d) in the regions adjacent to the dike or sill, and 3) the closing of cracks and pore space by thermal annealing due to conductive heating and viscous deformation adjacent to the sill or dike. Kiefer (2013) concluded that thermal annealing of the porous feldspathic host rock could substantially reduce the host rock porosity and allow a large volume of magma to be intruded into the lunar crust with little overall change in crustal volume. This thermal annealing mechanism, according to Kiefer (2013), could result in sills of substantial thickness (at least 3-6 km in the cases considered in the Marius Hills) being intruded into the upper crust without requiring any visible uplift deforming the surface (the uplift being offset by crack closure and porosity loss).

These considerations lead to fundamental questions about the influence of three aspects of magmatic processes on shallow crustal structure: 1) the role of “micro-intrusions” into the more porous and permeable material surrounding dikes and sills (shallow magmatic percolation), resulting in densification of the country rock; 2) the role of “thermal annealing” from the dike or sill intrusion in closing the fractures and densifying the adjacent country rock; 3) the effect these two processes would have on the topography and density structure of the crust; and 4) the role of the observed and interpreted crustal density structure in favoring the likelihood of “sill emplacement” at different depths within the lunar crust. These considerations are all critical to a proper understanding of the density structure of the lunar crust, the interpretation of gravity data, and the relation of shallow magma bodies to the surface geologic record. We address each of these in turn.

III. Processes:

1) Shallow Magmatic Percolation: Magma injection into pre-existing fractures: In an assessment of Lunar Prospector gravity data for the northern part of the Marius Hills region, Kiefer (2013) used maximum values for surface topography and still required a subsurface high-density layer of ~1.6-2.4 km thickness, depending on the density assumed. On the basis of the lack of evidence for a buried crater in this region, Kiefer (2013) proposed the presence of an upper crustal intruded sill of this thickness, but noted that this interpretation was not favored because of the absence of the corresponding crustal uplift and surface deformation that would be expected. In order to account for the vertical uplift induced by the intrusion of an ~1.6-2.4 km thick sill, clearly some alternative method of density offset is required. Kiefer (2013) called on “intrusion of magma in subsurface void space, primarily in the form of a connected network of cracks” to densify the intruded country rock and offset the need for vertical uplift. In the following paragraphs, we examine the role of “micro-intrusions” (typically known as apophyses) into the more porous and permeable material surrounding dikes and sills, resulting in densification of the country rock. On the basis of the envisioned process of “intrusion of magma in subsurface void space”, we describe this as “shallow magmatic percolation”, which we distinguish from magmatic percolation in deep partially melted magma source regions (see Vigneresse et al., 1996, for quantitative descriptions of these source region rheological transitions) or gaseous percolation in shallower regions.

In order to assess the importance of shallow magmatic percolation (Figure 2a) we model fractures of various mean widths W and inject lunar magma with viscosity η under a pressure gradient of the same order as buoyancy, $\mathrm{d}P/\mathrm{d}z = g\, \Delta\rho$ where $\Delta\rho = 300$ kg m^{-3}. Lunar magmas have low viscosities compared with terrestrial basalts and may initially move in a turbulent fashion even when injected into narrow fractures. This results in efficient heat transfer to the walls of the fracture, rapid cooling, the progressive formation of crystals, and the onset of non-Newtonian rheology. We therefore assume that in general the magma being injected has a yield strength Y that depends on the current crystal volume fraction f_c such that

$$Y = 0 \quad , f_c < f_0 \qquad (1a)$$

$$Y = A\ \{[(f_c/f_0) - 1]/[1 - (f_c/f_m)]\}^p \quad , f_c > f_0 \qquad (1b)$$

where $A = 2.95 \times 10^{-4}$ Pa, $f_m = 0.45$, $p = 3.509$, and the onset of a yield strength occurs at $f_0 = 0.021$ (Ishibashi and Sato, 2010). The crystal fraction is assumed to increase linearly as the temperature decreases from the liquidus T_l to the solidus T_s:

$$f_c = (T_l - T) / (T_l - T_s) \qquad (2)$$

The temperature-dependent viscosity, η, of crystal-free lunar basalt is well-approximated by a power law (Hulme, 1973; 1982) and fitting the viscosity data for a low-Ti mare basalt analyzed by Williams et al. (2000) gives

$$\eta = (1582.21 / T)^{11.5826} \qquad (3)$$

The bulk viscosity is then related to the liquid viscosity via a correction factor f_v:

$$\eta_b = f_v\ \eta \qquad (4)$$

where

$$f_v = [1 - (f_c / 0.6)]^{-2.5} \quad , f_c < 0.3 \qquad (5a)$$

$$f_v = \exp\{[2.5 + (f_c /(0.6 - f_c))^{0.48}]\ (f_c / 0.6)\} \quad , f_c > 0.3 \qquad (5b)$$

Equation (5a) is the Roscoe-Einstein equation (Roscoe, 1952) and equation (5b) is given by Pinkerton and Stevenson (1992).

Standard fluid mechanics formulae (e.g., Knudsen and Katz, 1958) then give the flow speed of the magma as

$$U = (2 + q)\ (1 - q)^2\ [(W^2\ \mathrm{d}P/\mathrm{d}z) / (3\ \eta_b)] \qquad (6)$$

when the magma motion is laminar and

$$U = [(W\ \mathrm{d}P/\mathrm{d}z) / (f\ \rho)]^{1/2} \qquad (7)$$

when the motion is turbulent, where f is a friction factor close to 10^{-2}, ρ is the magma density, ~3000 kg m^{-3}, and q is defined as

$$q = Y / (W \, dP/dz) \tag{8}$$

An initially turbulent fluid will make the transition to laminar motion when the Reynolds number, Re, defined by

$$Re = (4 \, U \, W \, \rho) / \eta_b \tag{9}$$

decreases below some critical value, Re_{crit}, determined by the current value of the Hedström number, He, defined by

$$He = (16 \, W^2 \, Y \, \rho) / \eta_b^2 \tag{10}$$

The critical relationships is then well-approximated by

$$\log_{10} Re_{\mathrm{crit}} = 1.6 + 0.476 \log_{10} He \tag{11}$$

While motion is turbulent, heat is transferred from the magma at temperature T to the walls of the fracture at temperature T_a at a rate per unit area H given by

$$H = 0.023 \, (k/W) \, Pr^{0.4} \, Re^{0.8} \, (T - T_a) \tag{12}$$

where k is the thermal conductivity of the host rock and Pr is the Prandtl number:

$$Pr = h_b / (\rho \, \kappa) \tag{13}$$

where κ is the thermal diffusivity of lava, ~10^{-6} m^2 s^{-1}. The heat loss causes a decrease in the lava temperature by an amount ΔT while the lava advances a distance Δz such that

$$\Delta T = (H \, \Delta z) / (\rho \, c \, W \, U) \tag{14}$$

where c is the specific heat of the lava. For cases where the initial magma motion is turbulent we use equations (12)-(14) to track the decreasing temperature. Cooling leads to increases in Y, η_b, He and Re_{crit}. The increases in η_b and Y causes U to decrease, and so the initially high Reynolds number Re decreases until it intersects the increasing Re_{crit} and the motion becomes laminar. We note the distance that the magma has travelled when this occurs, Z_t. From this point onward thermal boundary layers grow against the walls of the fracture, and motion stops when the two boundary layers meet in the center of the flow. This criterion is the basis of the Grätz number treatment for the maximum travel distances of laminar lava flows (Pinkerton and Wilson, 1994), and adapting it to flow in a planar fracture we find the maximum additional distance that the magma can advance, Z_l, where

$$Z_l = (U \, W^2) / (Gz \, \kappa) \tag{15}$$

and *Gz* is the critical Grätz number, ~300. The maximum penetration distance of magma into the fracture is then Z_m where

$$Z_m = Z_t + Z_l \tag{16}$$

Table 1 shows the values of Z_t, Z_l and Z_m for magma injections into fractures with widths, *W*, from 1 cm to 1 m and Figure 2b shows the relationship between Z_m and *W* graphically. The penetration distance increases dramatically for fractures more than a few tens of cm wide. However, there is little evidence that such wide fractures will exist in the lunar crust. Fractures are extremely common at the 10-20 μm scale in impact-modified rocks (Kenkmann et al, 2014). Drilling at Chicxulub crater revealed porosities between 5 and 24% (Elbra and Pesonen, 2011). Gravity data from many terrestrial craters (Ries, Tvären, and Granby) are interpreted as indicating porosities of less than 20% down to depths of 1-2 km (Pohl et al., 1977; Henkel et al., 2010), similar to porosities of lunar rocks (Kiefer et al., 2012) and the bulk lunar crust (Wieczorek et al., 2013; Besserer et al., 2014). Exposures at the Vredefort impact structure (Lieger et al., 2009, 2011) suggest that at larger scales the commonest fracture width is in the range 1-3 cm. In summary, lunar magmas driven by the pressure gradients expected for volcanic intrusions would penetrate less than 1 m in cracks of such scale (Figure 2b).

Very near-surface Hawaiian rift zone dike intrusions sometimes result in void space in the upper several tens to a very few hundreds of meters of the crust (e.g., Johnson et al., 2010), as magma drains at the distal, downslope end of the dike system at the end of an eruption, but this effect is limited to the very near surface in laterally emplaced dikes, in coherent rocks such as basalt that can support an open crack. Such open cracks are not anticipated on the Moon due to the lack of shallow magma reservoirs feeding large shield volcanoes and their associated lateral dike systems (Head and Wilson, 1991) and also due to the fact that most vertical dikes from the mantle are emplaced in the highlands megaregolith, a fragmental layer disfavoring maintaining wide open cracks. Exceptions on the Moon might be the upper parts of dikes that penetrate to the near surface and then undergo gas loss (e.g., pit crater chains; Head and Wilson, 2017) or summit pit craters on shield volcanoes that are predicted to be very porous in the upper several hundred meters (e.g., Qiao et al., 2017, 2018; Wilson and Head, 2017b). However, such wide cracks are unlikely to occur below a few tens to hundreds of meters due to closure from overburden pressure.

In summary, on the Moon magmatic percolation should not be common at distances greater than a few tens of cm from the edge of an intruding dike or sill, and since the majority of cracks are predicted to be in the 10-20 μm range (Figure 2b), where the amount of intrusion is very small, the cumulative effect of magmatic percolation on the density structure should be negligible.

2) Thermal Annealing: Consequences of dike and sill intrusions:

As described above, Wieczorek et al. (2013) called on gravitational loading of crustal rock deforming with a strongly temperature-dependent viscosity to cause densification at a minimum depth estimated to be ~40 km (Figure 1b). On the other hand, penetration of dikes to the shallow crust and surface and potential intrusion of shallow sills (as in the case proposed by Keifer, 2013) should also be accompanied by thermal annealing. We now consider such a case to assess the importance of thermal annealing and its role in changing the density structure adjacent to an intruded basaltic sill, and potentially influencing the gravity signature and the magnitude of the surface topographic uplift.

The thermal consequences of the abrupt injection of a sill into much cooler rocks can be modelled analytically using treatments by Carslaw and Jaeger (1959). For the present case the most useful approximation is a horizontal sheet of magma at temperature T_m emplaced rapidly into an infinitely extensive body of host rock at temperature T_a (Figure 3a). If the vertical half-thickness of the sill is a, the temperature T as a function of time t and vertical distance z from the center of the sill is (Carslaw and Jaeger, 1959, article 2.4.i)

$$T = T_a + 0.5\,(T_m - T_a)\,\{\mathrm{erf}\,[(a - z) / \lambda + \mathrm{erf}\,[(a + z) / \lambda]\} \qquad (17)$$

where

$$\lambda = 2\,(\kappa\, t)^{1/2} \qquad (18)$$

For cases where the top of the sill is at a depth less than or comparable to the thickness of the sill an alternative analytical solution approximating to the geometry would be that in article 2.4.iv of Carslaw and Jaeger (1959), in which the top of the sill would be exactly at the planetary surface. In practice, both treatments yield essentially the same results for the penetration of heat from the sill into the country rocks.

A number of simple relationships emerge (Figure 3b). First, the interface between the sill and the host rocks almost instantly reaches a temperature that is the average of the temperatures of the magma and host. The highest liquidus temperature for a lunar magma reported by Williams et al. (2000) is 1440 °C, i.e., 1713 K, for a low-Ti basalt. A representative thermal conductivity for lunar crustal rocks is ~1.3 W m^{-1} K^{-1} (Robertson, 1988) and the lunar geothermal heat flow is ~3 × 10^{-2} W m^{-2} (Vanimann et al., 1991). With an average surface ambient temperature of ~250 K, the temperature at a depth of ~10 km in the Moon will be ~480 K; injection of the above magma will lead to an interface temperature of 1097 K, i.e., 824 °C. Kiefer (2013) quotes data from Simonds (1973) and Uhlmann et al. (1975) showing that lunar rocks experienced substantial annealing if held at >800 °C for the order of a year. Heat transfer from a sill to its host rocks will occur on a much longer time scale, but the peak temperature experienced by the host rocks will decrease approximately exponentially with distance from the sill margin, and a given temperature will be experienced for a duration that increases as the square of the sill thickness. Our model conservatively assumes that a temperature of 700 °C is needed for efficient annealing. Kiefer's (2013) gravity models imply that sills up to 6 km in thickness might be needed to explain the gravity data he analyzed. Using this extreme sill thickness in our model, we find that the 700 °C isotherm extends for 600 m into the host rock for a period of ~250,000 years. If this results in complete elimination of, say, 30% pore space in these host rocks, both above and below the sill, the crust overlying the area of the sill intrusion would subside by ~360 m, 6% of the sill thickness. For a 3 km thick sill the corresponding values have the 700 °C isotherm extending for 300 m into the host rock for a period of ~30,000 years and again producing subsidence equal to 6% of the sill thickness. It is of course the case that greater volumes of crust are heated to lower temperatures than 700 °C for longer times but, given that we have used the highest plausible magma temperature, a very high initial porosity, and a conservative annealing temperature, we cannot see a situation where annealing would eliminate more than a small fraction of the topographic signature of the intrusion. For comparison (Figure 3a), the subsequent amount of topographic decrease due to sill cooling and solidification (~10%) is larger than the effect due to thermal annealing.

3) Intrusion of shallow dikes versus sills: Recent developments in the knowledge of lunar crustal thickness and density structure have enabled important revisions to models of the generation, ascent and eruption of magma, and new knowledge about the presence and behavior of magmatic volatiles has provided additional perspectives on shallow intrusion processes. Wilson and Head (2017a; 2018a, b) and Head and Wilson (2017) used these new data to assess the processes that occur during dike and sill emplacement. 1) The overpressurization values in deep basaltic magma source regions necessary to propagate a dike to the surface are sufficiently high that the repose time between dike emplacement events is likely to be measured in tens of thousands of years, an insufficient rate of intrusion to shallow depths to form shallow crustal magma reservoirs composed of multiple, still-molten dikes (Head and Wilson, 1991). 2) In contrast to small dike volumes and low dike propagation velocities in terrestrial environments, lunar dike propagation velocities are typically sufficiently high that shallow sill formation is not favored; local low-density breccia zones beneath impact crater floors, however, may provide a large enough material property contrast to cause lateral magma migration to form laccoliths (e.g., Vitello Crater) and sills (e.g., Humboldt Crater) in floor-fractured craters (Jozwiak et al., 2012, 2015, 2017) (Figure 4). Dynamical considerations (Wilson and Head, 2018a) lead to the conclusion that lunar dike magma volumes are up to ~1100 km^3, and are generally insufficient to form FFCs on the lunar farside; the estimated magma volumes available for injection into sills on the lunar nearside (up to ~800 km^3) are comparable to the observed floor uplift in many smaller FFCs, and thus consistent with these FFCs forming from a single dike emplacement event. Larger FFCs may form from multiple shallow sill intrusions (Jozwiak et al., 2017; Wilson and Head, 2018a).

In summary, on the basis of dynamics of dike emplacement and shallow crustal structure, dikes are by far the most abundant type of intrusion likely to occur in the lunar crust. Sills should be relatively uncommon except in local circumstances, such as floor-fractured craters.

IV Discussion and Conclusions:

On the basis of new data from the GRAIL mission that reveal lower density and higher porosity of crustal materials than previously interpreted, and recent models of the generation, ascent and eruption of basaltic magmatic dikes in and through the lunar crust, we have revisited the nature of magmatic intrusions in terms of the likelihood of shallow sill formation and the effects accompanying these processes, specifically, shallow magmatic percolation and thermal annealing (Figure 5).

Shallow Magmatic percolation: On the basis of the most plausible range of micro/macro-scale porosity and permeability (microns to a few cm) and open crack lateral continuity (mm to tens of cm), we have shown that rapid conductive cooling of injected magma, due to the very large surface area to volume ratio, restricts magmatic percolation to very limited distances (maximum several tens of cm) adjacent to the ascending dike or intruded sill, even in the upper several hundred meters of the lunar crust;

Thermal annealing: We find that the conductive heat loss from intruded dikes and sills results in a thermal wave decay pattern that is predicted to limit the effects of intrusion-adjacent thermal annealing to less than ~6% of the thickness of the intruded body (30 m on each side of a 1 km thick sill).

Difficulty of sill formation: The extremely rapid rise rate of magma in dikes derived from sources in the deep lunar mantle is not favorable to vertical dikes developing lateral off-shoots to form sills in the crust, except in specific shallow crustal environments influenced by impact crater-related environments (e.g., floor-fractured craters).

Influence of dike and sill intrusions on the gravity structure of the lunar crust and on surface topography: On the basis of these analyses we conclude that shallow magmatic percolation and thermal annealing in association with lunar mare basalt magmatic dike and sill emplacement should be taken into consideration in interpreting gravity signatures, but that the net effects are predicted to be minor. Magmatic percolation is found to induce a very slight increase in density of the country rock within a maximum of a few tens of cm of intrusion margins, a negligible effect from the perspective of GRAIL gravity data. Thermal annealing effects can induce a densification of country rock surrounding a dike or sill by elimination of pore space, but the effect is limited to a total area surrounding an intrusion having less than ~6% of the thickness of the intrusive sill. For example, for the 6 km sill intrusion envisioned by Keifer (2013) to explain a shallow gravity anomaly in the Marius Hills region (left side of Figure 5), thermal annealing would densify only about 360 m of adjacent material (~180 m on each side). This would offset only about 6% of the 6 km topographic uplift due to the intrusion, and similarly would offset only ~6% of the gravitational signature of the intrusion. In addition, the geometry of sill intrusion causing uplift of floor-fractured craters (Jozwiak et al., 2012, 2015, 2017; Wilson and Head, 2018a) clearly shows that thermal annealing does not substantially offset the influence of the intrusion on the density structure in those cases. Subsidence associated with cooling of the intrusive sill (about 10% of the sill thickness) (Figure 3a) (Wilson and Head, 2018a) is predicted to be more important than the thermal annealing process itself.

Implications for the Geometry of Shallow Crustal Intrusions Interpreted from Gravity Data: Positive Bouguer gravity anomalies in the crust have been attributed to: 1) positive topography on the crust-mantle boundary (e.g., Neumann et al., 2015), 2) lava filled buried craters (e.g., Evans et al., 2018; Huang et al., 2014), 3) sill intrusions beneath floor-fractured craters (e.g., Jozwiak et al., 2015, 2017; Head and Wilson, 2018a), 4) multi-km-thick sills intruded into the upper crust with the apparent excessive thickness of the sill offset by the magnitude of densification of the intruded crust by magmatic percolation and thermal annealing) (e.g., Kiefer, 2013), and 5) vertical dike complexes above a diapiric magma source region in the mantle (e.g. Head and Wilson, 2017). In the absence of evidence for a buried crater, floor-fractured crater, or crust-mantle boundary topography in association with a substantial positive Bouguer gravity anomaly, vertical dike complexes best explain the gravity anomalies (right side of Figure 5). They offer the advantage of throughgoing densification of the entire crust by solidified magma, with individual dikes often summing to 30-50% of the crust in volcanic complexes, without relying on additional densification mechanisms such as magmatic percolation and thermal annealing. Additionally, dike intrusion causes mainly lateral extension leading to small amounts of regional uplift, in contrast to sill intrusion that causes a much larger amount of local uplift (compare left and right sides of Figure 5).

Acknowledgments: We gratefully acknowledge funding to JWH for participation in the Lunar Reconnaissance Orbiter (LRO) Lunar Orbiter Laser Altimeter (LOLA) Experiment Team (Grants NNX11AK29G- National Aeronautics and Space Administration and Goddard NNX13AO77G - National Aeronautics and Space Administration - Goddard). Much of the synthesis work for this contribution was enabled by participation in the NASA Solar System Exploration Research Virtual Institute (JWH and LW), through the SEEED (SSERVI Evolution and Environment of Exploration Destinations) cooperative agreement number NNA14AB01A at Brown University. LW was supported by the Leverhulme Trust through an

Emeritus Fellowship. Thanks are extended to Greg Neumann for a helpful review and to Anne Côté for help in figure drafting and all stages of manuscript preparation.

References

Besserer, J., Nimmo, F., Wieczorek, M.A., Weber, R.C., Kiefer, W.S., McGovern, P. J., Andrews-Hanna, J.C., Smith, D.E., Zuber, M.T., 2014. GRAIL gravity constraints on the vertical and lateral density structure of the lunar crust. Geophys. Res. Lett. 41, 5771-5777, doi: 10.1002/2014GL060240.

Carslaw, H.S., Jaeger, J.C., 1959. *Conduction of Heat in Solids*. 2nd edition. Oxford University Press, 510 pp.

Elbra, T., Pesonen, L.J., 2011. Physical properties of the Yaxcopoil ‐ 1 deep drill core, Chicxulub impact structure, Mexico. Meteorit. Planet. Sci. 46, 1640-1652, doi: 10.1111/j.1945-5100.2011.01253.x.

Evans, A.J., Andrews-Hanna, J.C., Head III, J.W., Soderblom, J.M., Solomon, S.C., M.T. Zuber, 2018. Reexamination of early lunar chronology with GRAIL data: Terranes, basins, and impact fluxes. J. Geophys. Res. 123, 1596-1617, doi: 10.1029/2017JE005421.

Han, S.-C., Schmerr, N., Neumann, G., Holmes, S., 2014. Global characteristics of porosity and density stratification within the lunar crust from GRAIL gravity and Lunar Orbiter Laser Altimeter topography data. Geophys. Res. Lett. 41, 1882-1889, doi: 10.1002/2014GL059378.

Head, J.W., Wilson, L., 1991. Absence of large shield volcanoes and calderas on the Moon: Consequence of magma transport phenomena? Geophys. Res. Lett. 18, 2121-2124.

Head, J.W., Wilson, L., 1992. Lunar mare volcanism: Stratigraphy, eruption conditions, and the evolution of secondary crusts. Geochim. Cosmochim. Acta 55, 2155-2175.

Head, J.W., Wilson, L., 2017. Generation, ascent and eruption of magma on the Moon: New insights into source depths, magma supply, intrusions and effusive/explosive eruptions (part 2: observations). Icarus, 283, 176-223, doi: 10.1016/j.icarus.2016.05.031.

Head, J.W., Wilson, L., 2018a

Henkel, H., Ekneligoda, T.C., Aaro, S., 2010. The extent of impact induced fracturing from gravity modeling of the Granby and Tvären simple craters. Tectonophysics 485, 290-305.

Huang, Q., Xiao, Z., Long, X., 2014. Subsurface structures of large volcanic complexes on the nearside of the Moon: A view from GRAIL gravity. Icarus 243, 48-57.

Hulme, G., 1973. Turbulent lava flow and the formation of lunar sinuous rilles. Modern Geology 4, 107-117.

Hulme, G., 1982. A review of lava flow processes related to the formation of lunar sinuous rilles. Geophysical Surveys 5, 245-279.

Ishibashi, H., Sato, H., 2010. Bingham fluid behavior of plagioclase-bearing basaltic magma: reanalyses of laboratory viscosity measurements for Fuji 1707 basalt. Journal of Mineralogical and Petrological Sciences 105, 334-339.

Johnson, D.J., Eggers, A.A., Bagnardi, M., Battaglia, M., Poland, M.P., Miklius, A., 2010. Shallow magma accumulation at Kilauea Volcano, Hawaii, revealed by microgravity surveys. Geology 38, 1139-1142.

Jozwiak, L.M., Head, J.W., Zuber, M.T., Smith, D.E., Neumann, G.A., 2012. Lunar floor-fractured craters: Classification, distribution, origin and implications for magmatism and shallow crustal structure. J. Geophys. Res. 117, E11005, doi: 10.1029/2012JE004134.

Jozwiak, L.M., Head, J.W., Wilson, L., 2015. Lunar floor-fractured craters as magmatic intrusions: Geometry, modes of emplacement, associated tectonic and volcanic features, and implications for gravity anomalies. Icarus 248, 424-447, doi: 10.1016/j.icarus.2014.10.052.

Jozwiak, L.M., Head, J.W., Neumann, G.A., Wilson, L., 2017. Observational constraints on the identification of shallow lunar magmatism: Insights from floor-fractured craters. Icarus 283, 224-231, doi: 10.1016/j.icarus.2016.04.020.

Kenkmann, T., Poelchau, M.H., Wulf, G., 2014. Structural geology of impact craters. Journal of Structural Geology 62, 156-182.

Kiefer, W.S., 2013. Gravity constraints on the subsurface structure of the Marius Hills: The magmatic plumbing of the largest lunar volcanic dome complex. J. Geophys. Res. 118, 733-745, doi: 10.102/2012JE004111.

Kiefer, W.S., Macke, R.J., Britt, D.T., Irving, A.J., Consolmagno, G.J., 2012. The density and porosity of lunar rocks. Geophys. Res. Lett. 39, L07201, doi: 10.1029/2012GL051319.

Knudsen, J.G., Katz, D.L., 1958. Fluid Dynamics and Heat Transfer. McGraw-Hill, New York. 576 pp.

Lieger, D, Riller, U., Gibson, R.L., 2009. Generation of fragment-rich pseudotachylite bodies during central uplift formation in the Vredefort impact structure, South Africa. Earth Planet. Sci. Lett. 279, 53-64.

Lieger, D, Riller, U., Gibson, R.L., 2011. Petrographic and geochemical evidence for an allochthonous, possibly impact melt, origin of pseudotachylite from the Vredefort Dome, South Africa. Geochim. Cosmochim. Acta 75, 4490-4514.

Lognonné, P., Gagnepain-Beyneix, J., Chenet, H., 2003. A new seismic model of the Moon: implications for structure, thermal evolution and formation of the Moon. Earth Planet. Sci. Lett. 211, 27-44, doi: 10.1016/S0012-821X(03)00172-9.

Neumann, G.A., Zuber, M.T., Wieczorek, M.A., J.W. Head III, Baker, D.M.H., Solomon, S.C., Smith, D.E., Lemoine, F.G., Mazarico, E., Sabaka, T.J., Goossens, S., Melosh, H.J., Phillips, R.J., Asmar, S.W., Konopliv, A.S., Williams, J.G., Sori, M.M., Soderblom, J.M., Miljkovic, K., Andrews-Hanna, J.C., Nimmo, F., Kiefer, W.S., 2015. Lunar impact basins revealed by Gravity Recovery and Interior Laboratory measurements. Science Advances 1, 1-10, doi: 10.1126/sciadv.1500852.

Pinkerton, H., Stevenson, R.J.,1992. Methods of determining the rheological properties of magmas at sub-liquidus temperatures. J .Volcanol. Geotherm. Res. 53, 47-66.

Pinkerton, H., Wilson, L., 1994. Factors controlling the lengths of channel-fed lava flows. Bull. Volcanol. 56 (2), 108-120.

Pohl, J. Stoeffler, D., Gall, H. Ernstson, K., 1977. The Reis impact crater, in: Roddy, D.J., Pepin, R.O., Merrill, R.B. (Eds.), Impact and Explosion Cratering: Planetary and Terrestrial Implications. Pergamon Press, New York, pp. 343-404.

Qiao, L., Head, J.W., Wilson, L., Xiao, L., Dufek, J.D., 2017. Ina pit crater on the Moon: Extrusion of waning-stage lava lake magmatic foam results in extremely young crater retention ages. Geology 45, 455-458, doi: 10.1130/G38594.1.

Qiao, L., Head, J.W., Xiao, L.,Wilson, L., Dufek, J.D.. 2018. The role of substrate characteristics in producing anomalously young crater retention ages in volcanic deposits on the Moon: Morphology, topography, subresolution roughness, and mode of emplacement of the Sosigenes lunar irregular mare patch. Meteoritics and Planetary Science 53, 778-812, doi: 10.1111/maps.13003.

Robertson, E.C., 1988. Thermal properties of rocks. U.S. Geological Survey Open File Report 88-441, 106 pp.

Roscoe, R., 1952. The viscosity of suspensions of rigid spheres. British Journal of Applied Physics 3, 267–269.

Shearer, C.K., Hess, P.C., Wieczorek, M.A., Pritchard, M.E., Parmentier, E.M., Borg, L.E., Longhi, J., Elkins-Tanton, L.T., Neal, C.R., Antonenko, I., Canup, R.M., Halliday, A.N., Grove, T.L., Hager, B.H., Lee, D.-C., Wiechert, U., 2006. Thermal and Magmatic Evolution of the Moon, in: Jolliff, B.L., Wieczorek, M.A., Shearer, C.K, Neal, C.R. (Eds.), New Views of the Moon, Reviews in Mineralogy and Geochemistry 60, p. 365 – 518.

Simonds, C.H., 1973. Sintering and hot pressing Fra Mauro composition glass and the lithification of lunar breccias. Am. J. Sci. 273, 428-439.

Soderblom, J.M., Evans, A.J., Johnson, B.C., Melosh, H.J., Miljkovic, K., Phillips, R.J., Andrews-Hanna, J.C., Bierson, C.J., Head III, J.W., Milbury, C., Neumann, G.A., Nimmo, F., Smith, D.E., Solomon, S.C., Sori, M.M., Wieczorek, M.A., Zuber, M.T., 2015. The fractured Moon: Production and saturation of porosity in the lunar highlands from impact cratering. Geophys. Res. Lett. 42, 6939-6944, doi: 10.1002/2015GL065022.

Uhlmann, D.R., Klein, L., Onorato, P.I.K., Hopper, R.W., 1975. The formation of lunar breccias: Sintering and crystallization kinetics. Proc. Lunar Sci. Conf. 6, 693-705.

Vaniman, D., Reedy, R., Heiken, G., Olhoeft, G., Mendell, W., 1991. The lunar environment, in: Heiken, G.H., Vaniman, D.T., French, B.M. (Eds.), The Lunar Source Book, Cambridge Univ. Press, pp. 27-60.

Vigneresse, J.L., Barbey, P., Cuney, M., 1996. Rheological transitions during partial melting and crystallization with application to felsic magma segregation and transfer. J. Petrology 37, 1579-1600.

Wieczorek, M.A., Jolliff, B.L., Khan, A., Pritchard, M.E., Weiss, B.P., Williams, J.G., Hood, L.L., Righter, K., Neal, C.R., Shearer, C.K., McCallum, I.S., Tompkins, S., Hawke, B.R., Peterson, C., Gillis, J.J., Bussey, B., 2006. The constitution and structure of the lunar interior, in: Jolliff, B.L., Wieczorek, M.A., Shearer, C.K, Neal, C.R. (Eds.), New Views of the Moon, Reviews in Mineralogy and Geochemistry 60, p. 221-364.

Wieczorek, M.A., Neumann, G.A., Nimmo, F., Kiefer, W.S., Taylor, G.J., Melosh, H.J., Phillips, R.J., Solomon, S.C., Andrews-Hanna, J.A., Asmar, S.W., Konopliv, A.S., Lemoine, F.G., Smith, D.E., Watkins, M.M., Williams, J.G., Zuber, M.T., 2013. The crust of the Moon as seen by GRAIL. Science 339, 671-675, doi: 10.1126/science.1231530.

Williams, D.A., Fagents, S.A., Greeley, R., 2000. A reevaluation of the emplacement and erosional potential of turbulent, low-viscosity lavas on the Moon. J. Geophys. Res. 105, 20,189–20,206.

Wilson, L., Head, J.W., 1981. Ascent and eruption of basaltic magma on the Earth and Moon. J. Geophys. Res. 86 (B4), 2971-3001.

Wilson, L., Head, J.W., 2017a. Generation, ascent and eruption of magma on the Moon: New insights into source depths, magma supply, intrusions and effusive/explosive eruptions (Part 1: Theory). Icarus 283, 146-175, doi: 10.1016/j.icarus.2015.12.039.

Wilson, L., Head, J.W., 2017b. Eruption of magmatic foams on the Moon: Formation in the waning stages of dike emplacement events as an explanation of "irregular mare patches". Journal of Volcanology and Geothermal Research 335, 113-127, doi: 10.1016/j.jvolgeores.2017.02.009.

Wilson, L., Head, J.W., 2018a. Lunar floor-fractured craters: Modes of dike and sill emplacement and implications of gas production and intrusion cooling on surface morphology and structure. Icarus 305, 105-122, doi: 10.1016/j.icarus.2017.12.030.

Wilson, L., Head, J.W., 2018b. Controls on lunar basaltic volcanic eruption structure and morphology: Gas release patterns in sequential eruption phases, Geophys. Res. Lett. 45, 5852-5859, doi: 10.1029/2018GL078327.

Wilson, L., Head, J.W., Zhang, F., 2019. A theoretical model for the formation of Ring Moat Dome Structures: Products of second boiling in lunar basaltic lava flows. J. Volcanology and Geothermal Research 374, 160-180, doi: 10.1016/j.jvolgeores.2019.02.018.

Zuber, M.T., Smith, D.E., Lehman, D.H., Hoffman, T.L., Asmar, S.W., Watkins, M.M., 2013. Gravity recovery and interior laboratory (GRAIL): Mapping the lunar interior from crust to core. Space Sci. Rev. 178, 3-24, doi: 10.1007/s11214-012-9952-7.

Figure Captions:

Figure 1. Lunar crustal structure. a. Factors influencing the density and porosity of the lunar crust throughout lunar history. Cooling and solidification of the initial crust, accompanied by and following impact bombardment, are the main factors in inducing crustal fractures and porosity. b. Three-tier structure of the lunar crust and processes operating to alter density and porosity at different depths. The upper megaregolith layer is composed primarily of allochthonous breccias (deformed, fragmented and transported bedrock at various scales), transitioning with depth to autochthonous breccias (formed *in situ* by fracturing, dilational bulking, injection of breccia dikes). At increasingly greater depths, overburden pressure closes fractures and cracks, and at the greatest depths in the crust (>~40 km), thermal annealing combines with overburden pressure to maximize closure of cracks and fractures.

Figure 2. The process of shallow magmatic percolation adjacent to dikes and sills in the crust. a) Shallow sill intrusion into the upper fractured lunar crust (left) and related processes of magma percolation immediately adjacent to the intrusion (right). Note that the zone of potential densification by magmatic percolation adjacent to the sill is relatively minor in terms of the density of cracks and void space, the rapidity of cooling of injected magma, and the distance that magma can travel before cooling and cessation of penetration. The scale of the penetration (right) is essentially invisible at the scale of the crustal sill intrusion (left) b) Variation of the maximum distance that magma can penetrate into a fracture before cooling halts its progress shown as a function of the fracture width (also see Table 1). Note that the vast majority of cracks are at the 10-20 μm scale in impact-modified rocks, and that fractures and pore space in the crust are at the mm to cm scale; thus, the penetration distance of apophyses (small intrusive features adjacent to and emanating from the sill margins) is typically well below a meter. Labeled box shows the commonest large-scale fracture width (1-3 cm) for the Vredefort impact structure (Lieger et al., 2009, 2011).

Figure 3. Shallow sill intrusion into the lunar crust and related processes of thermal annealing. a. Conceptual diagram of crack density and the effects of thermal annealing. 1. Background fractured and brecciated upper crust. 2. Intrusion of 1 km thick sill uplifts surface topography 1 km and induces conductive thermal wave above and below the sill. 3. High-temperature part of the thermal wave adjacent to the sill induces viscous flow and crack closure, causing densification of the affected crust over about 3% of sill thickness on each side of the sill; surface subsides about 60 m. 4. Solidification and cooling of the intruded sill cause about 10% shrinkage and about 100 m additional subsidence. b. Depth-time plot of thermal effects of intrusion on adjacent host rock. The distribution of temperature, T, within and underneath one half of the sill is shown as a function of position (vertical direction) and time (horizontal direction, time increasing to the right). The distribution is symmetric about the upper edge of the figure. Initial sill temperature is 1440 °C and host rock temperature is 207 °C. A wave of heating initially spreads into the host rock but eventually a wave of cooling spreads into the sill. Maximum temperature of host rock at contact is 824 °C. Color coding is red, T > 700 °C; yellow, 700 °C > T > 600 °C; green, 600 °C > T > 500 °C; white T < 500 °C. Temperature variation with depth scales with sill thickness; temperature variation with time at a given depth scales with the square of the sill thickness.

Figure 4. Processes related to the intrusion and evolution of a sill in a floor-fractured crater (from Wilson and Head, 2018b). a) Timeline for major events in the emplacement and evolution of a sill beneath a large floor-fractured crater. The dike emplacement and sill intrusion events are very rapid compared with the time needed for sill volatile evolution, and magma cooling until sill solidification. Time is in a log scale. b) Diagrammatic representation of the changes in floor elevation in a large floor fractured crater intruded by a sill. (Left) Pre-sill intrusion crater floor. (Middle-left) sill formation (~2 km thick in this case) causes floor uplift. (Middle-right) Volatile segregation causes additional sill thickening and potential floor uplift (~30 m); (Right) Cooling and solidification causes sill shrinkage and thickness reduction (~350 m), potentially manifested in crater floor deformation. Final crater floor surface above completely cooled ~2 km thick intruded sill should be ~320 m below initial sill intrusion and uplift elevation (+ 2 km intrusion, + 30 m from foam/gas layer, −350 m from cooling and solidification). Gas/foam layer effects should be added to our considerations in the analysis in this contribution.

Figure 5. Subsurface structure of volcanic complexes. Comparison of intrusive sill model (left) and intrusive dike model (right). In the sill intrusion model (after Kiefer, 2013), intrusion of the 6 km thick sill should induce substantial surface uplift, which is not observed. Mechanisms to offset the effects of this surface uplift and satisfy the gravity data include 1) shallow magma percolation, the intrusion of sill magma into cracks, pores and voids adjacent to the sill, and 2) thermal annealing, the closure of cracks, voids and pore spaces by heating and viscous annealing (Kiefer, 2013). In the analyses presented here, each of these two mechanisms is modeled and neither is found to have substantial effects on country rock densification and reduction of pore space, the combined effects being limited to less than 3% of the thickness of the sill on each side. Thus, a near-surface gravity anomaly due to the intrusion of a 6 km sill would typically require evidence for a large topographic uplift that would not be substantially offset by these candidate country rock densification processes. In the intrusive dike model (right), individual dikes just penetrate to the surface and feed small shields composed of cooling limited flows (Head and Wilson, 2017), collectively building a small topographic rise above the source region. Many dikes fail to reach the surface and solidify *in situ*. Each small shield is likely to represent an individual dike emplacement event and collectively, together with dikes that just fail to reach the surface, these solidified dikes can exceed 30-50 % of the crust in this region, creating a substantial Bouguer gravity anomaly without the complications of the intrusive sill model.

Table 1. Magma travel distance Z_t while flowing turbulently, subsequent travel distance Z_l after motion becomes laminar, and maximum total penetration distance Z_m for magma intruded into open fractures of width *W*.

W	Z_t/m	Z_l/m	Z_m/m
1 cm	-	0.01	0.01
3 cm	-	0.78	0.78
5 cm	-	6	6
7.5 cm	4	21	25
10 cm	12	42	54
15 cm	32	117	149
20 cm	57	235	292
25 cm	86	420	506
30 cm	118	652	770
50 cm	267	2,300	2,567
1 m	750	11,000	11,750

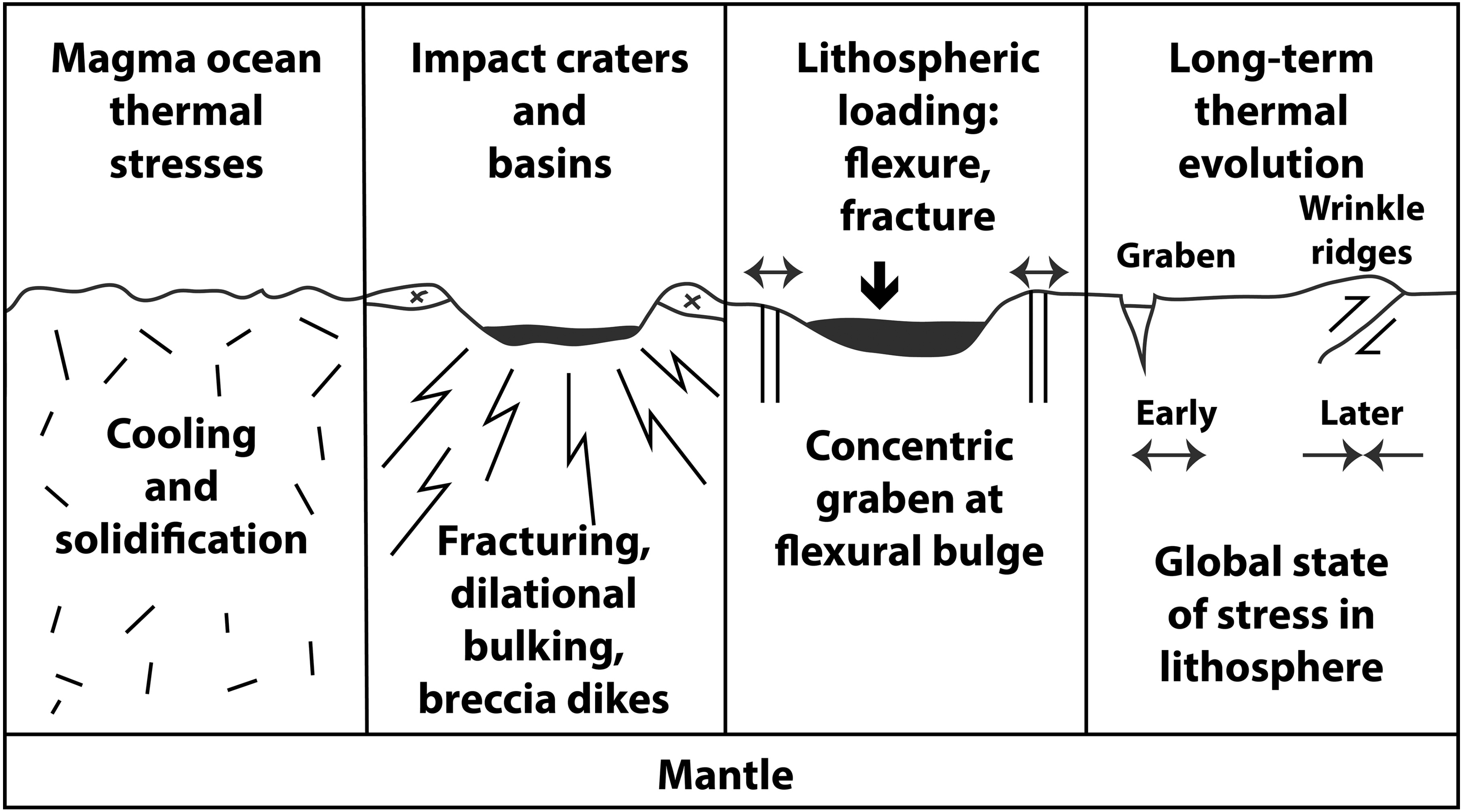

Figure 1a
5391
04/08/19

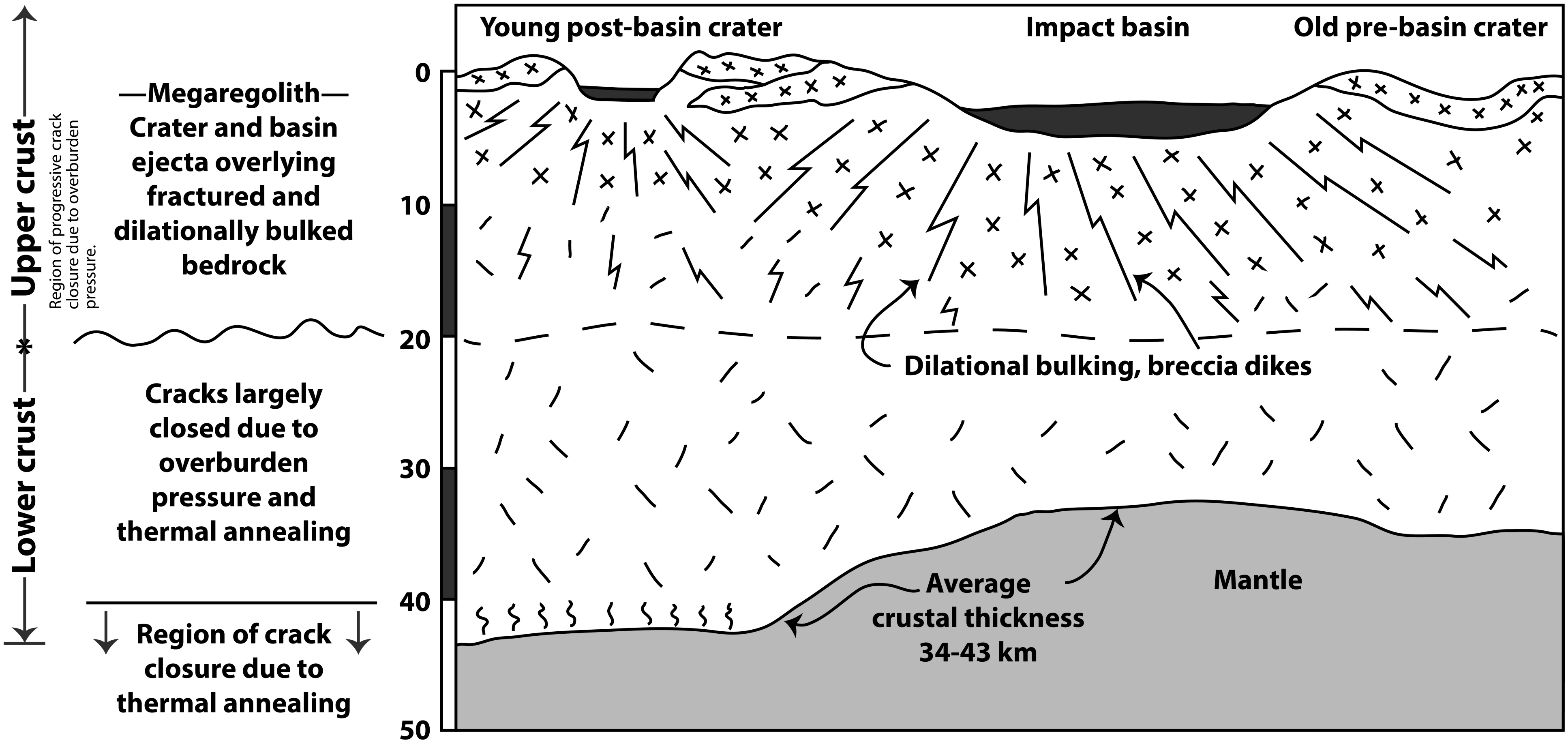

Figure 1b
5391
04/08/19

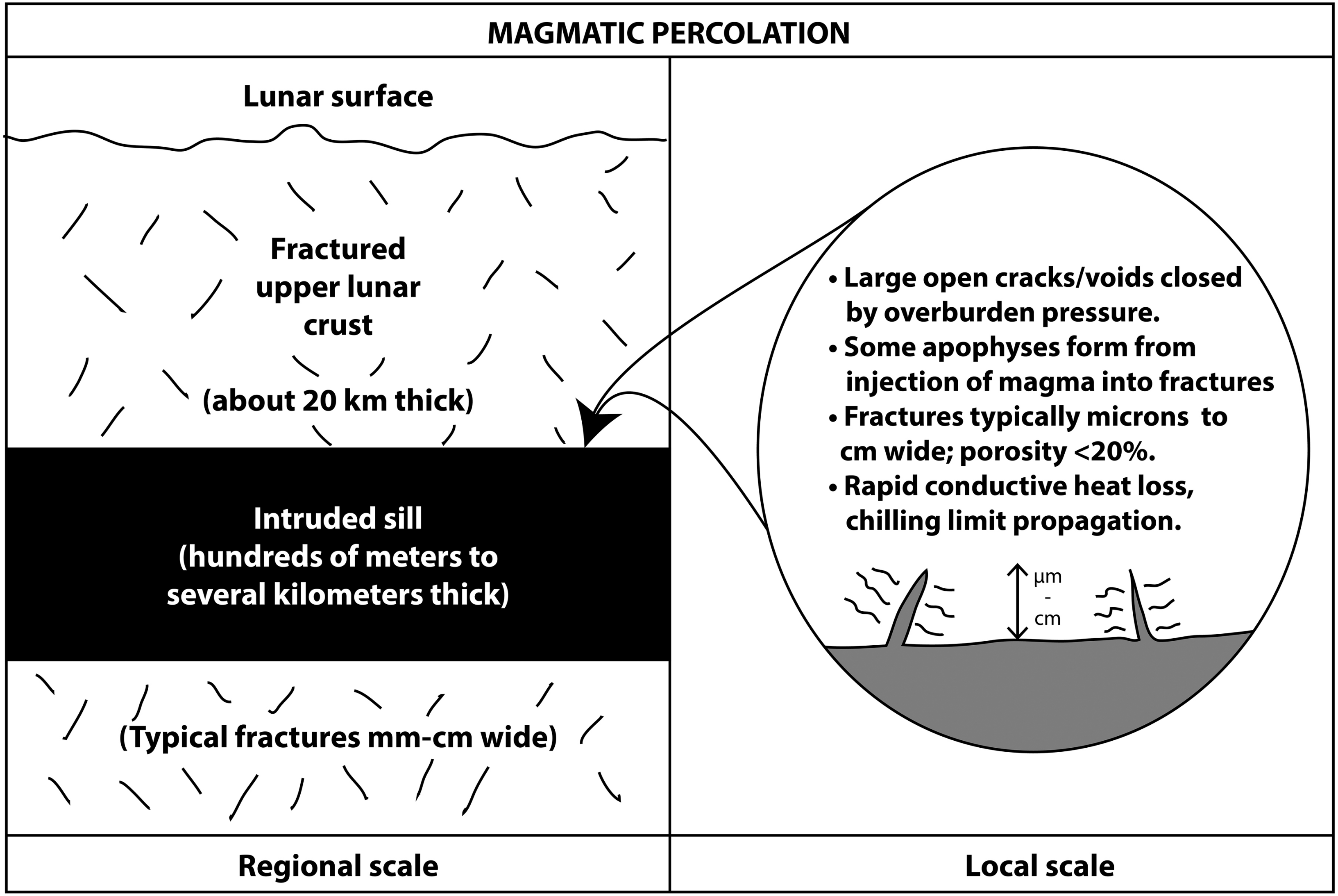

Figure 2a
5391
04/04/19

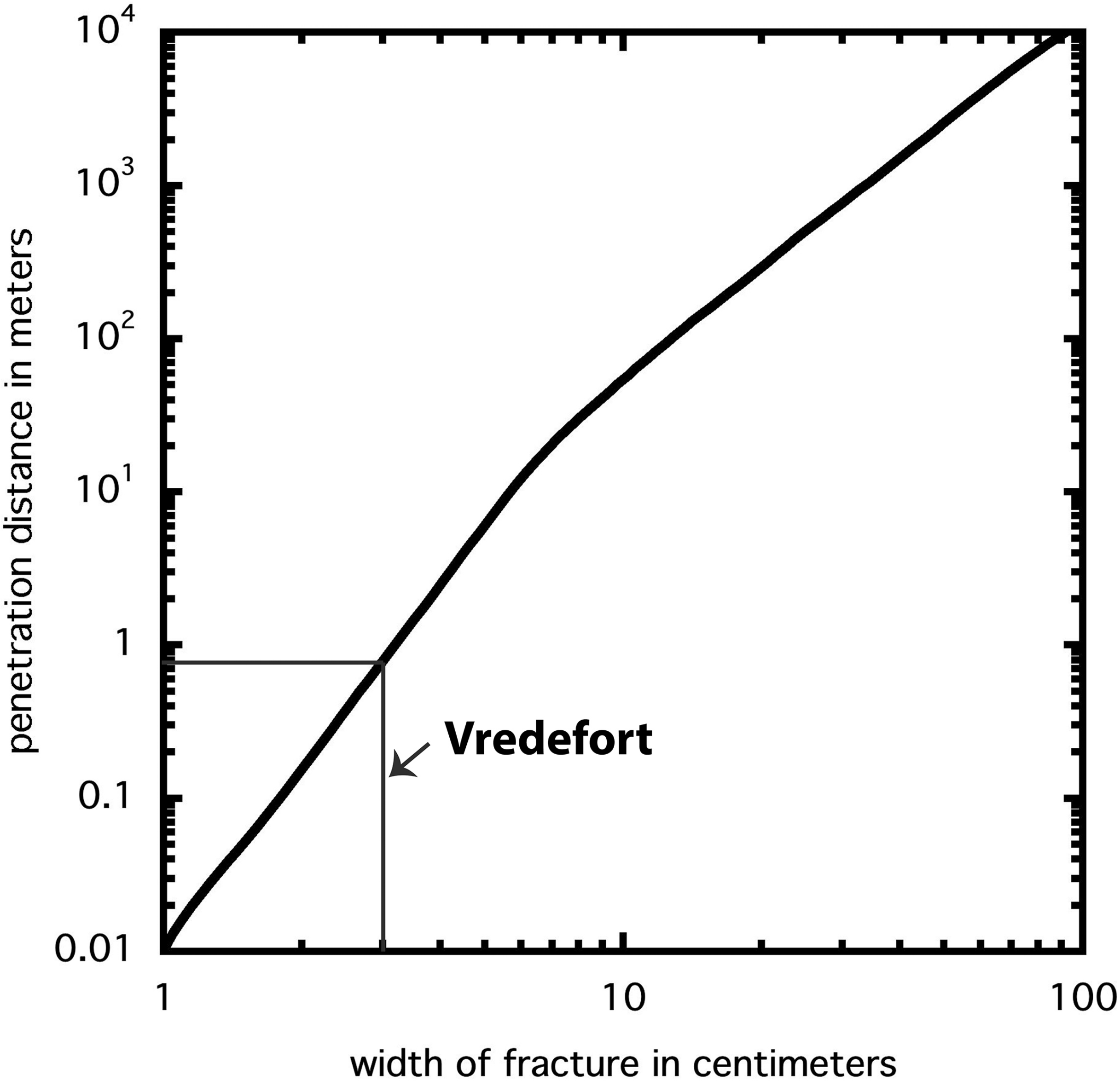

Figure 2b
5391
04/08/19

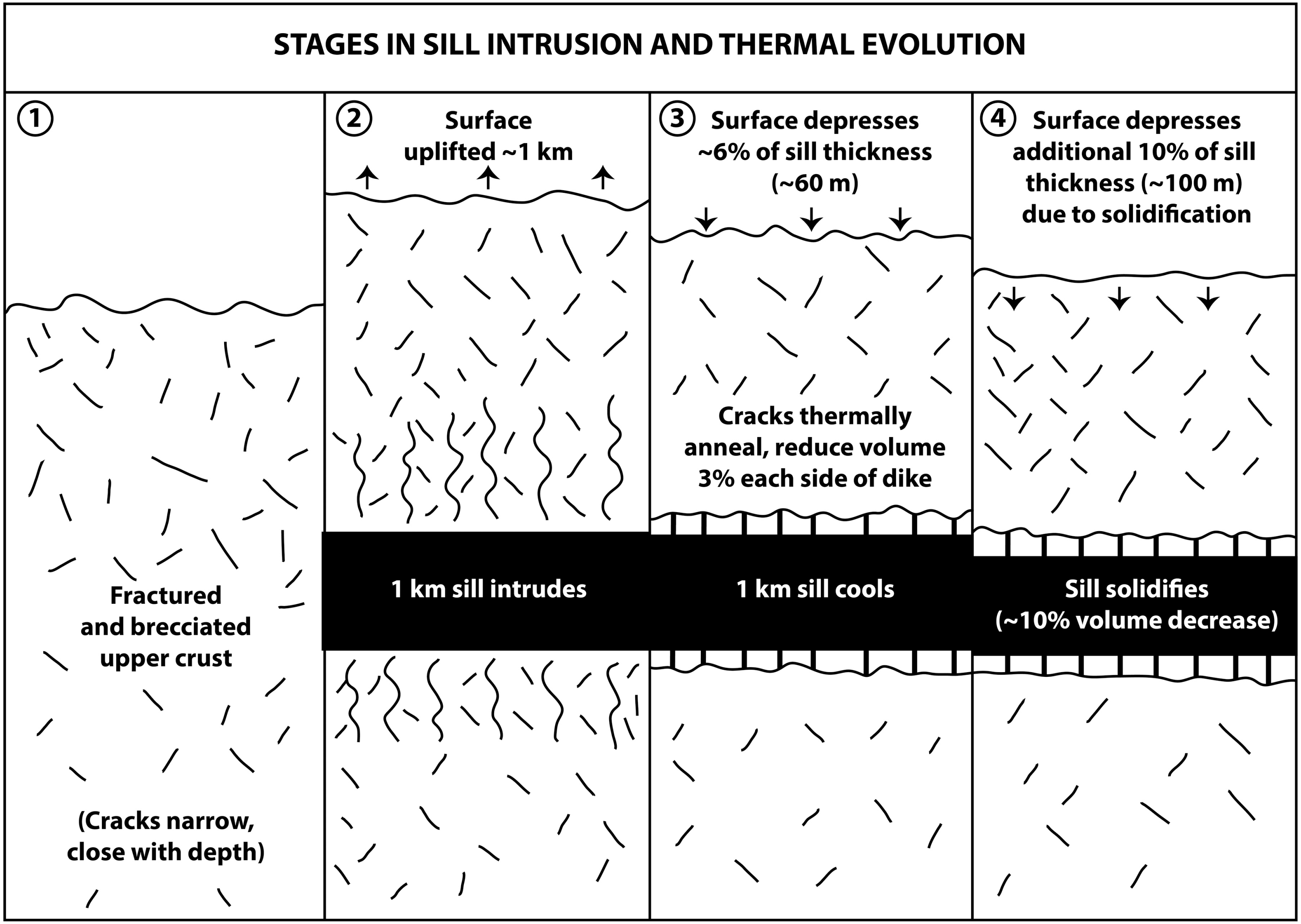

Figure 3a
5391
04/08/19

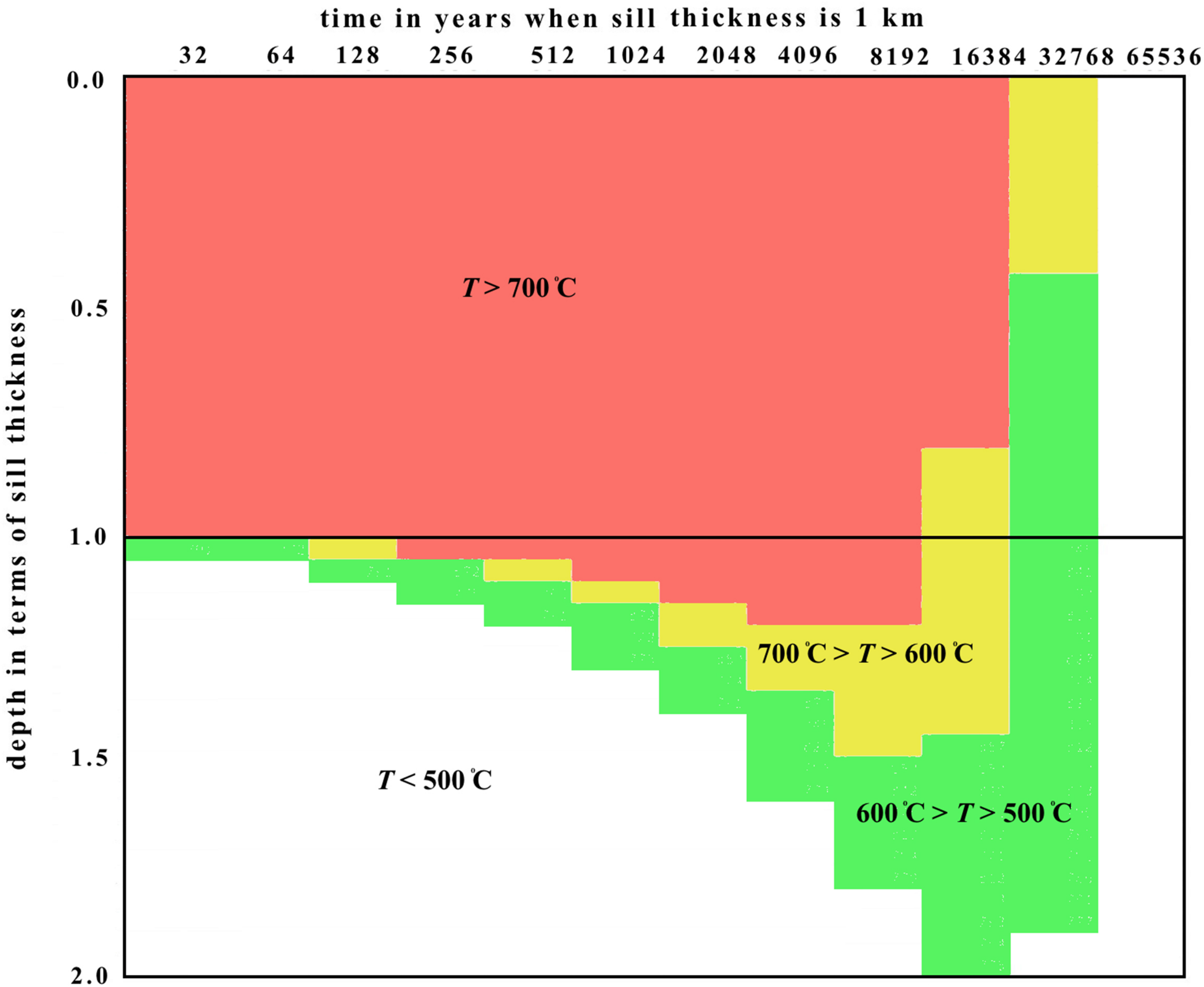

time in years when sill thickness is 1 km
32
64
128
256
512
1024
2048
4096
8192
16384
32768
65536
depth in terms of sill thickness
0.0
0.5
1.0
1.5
2.0
T > 700 ℃
700 ℃ > T > 600 ℃
600 ℃ > T > 500 ℃
T < 500 ℃

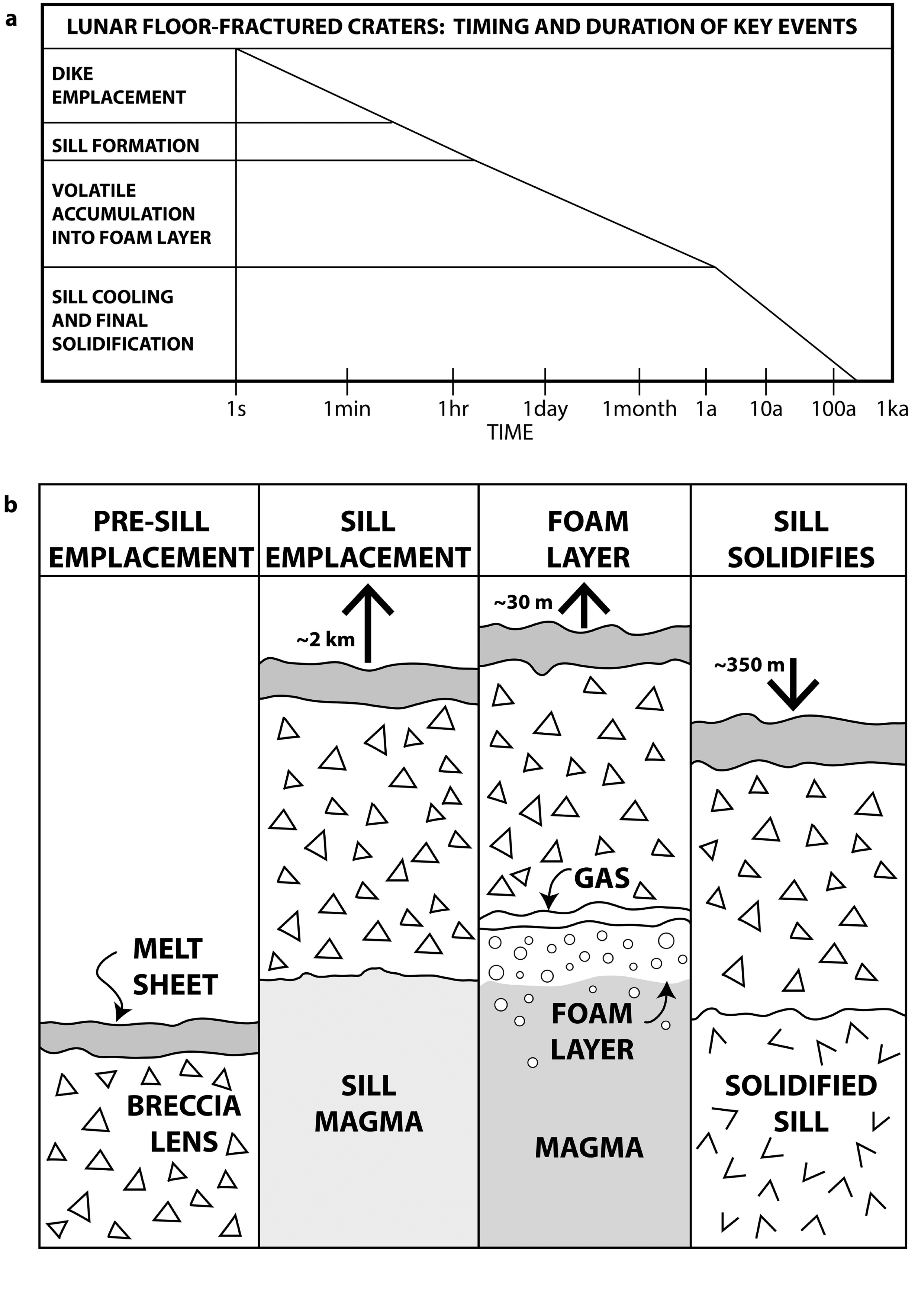

Figure 4a, b
5319
04/08/19

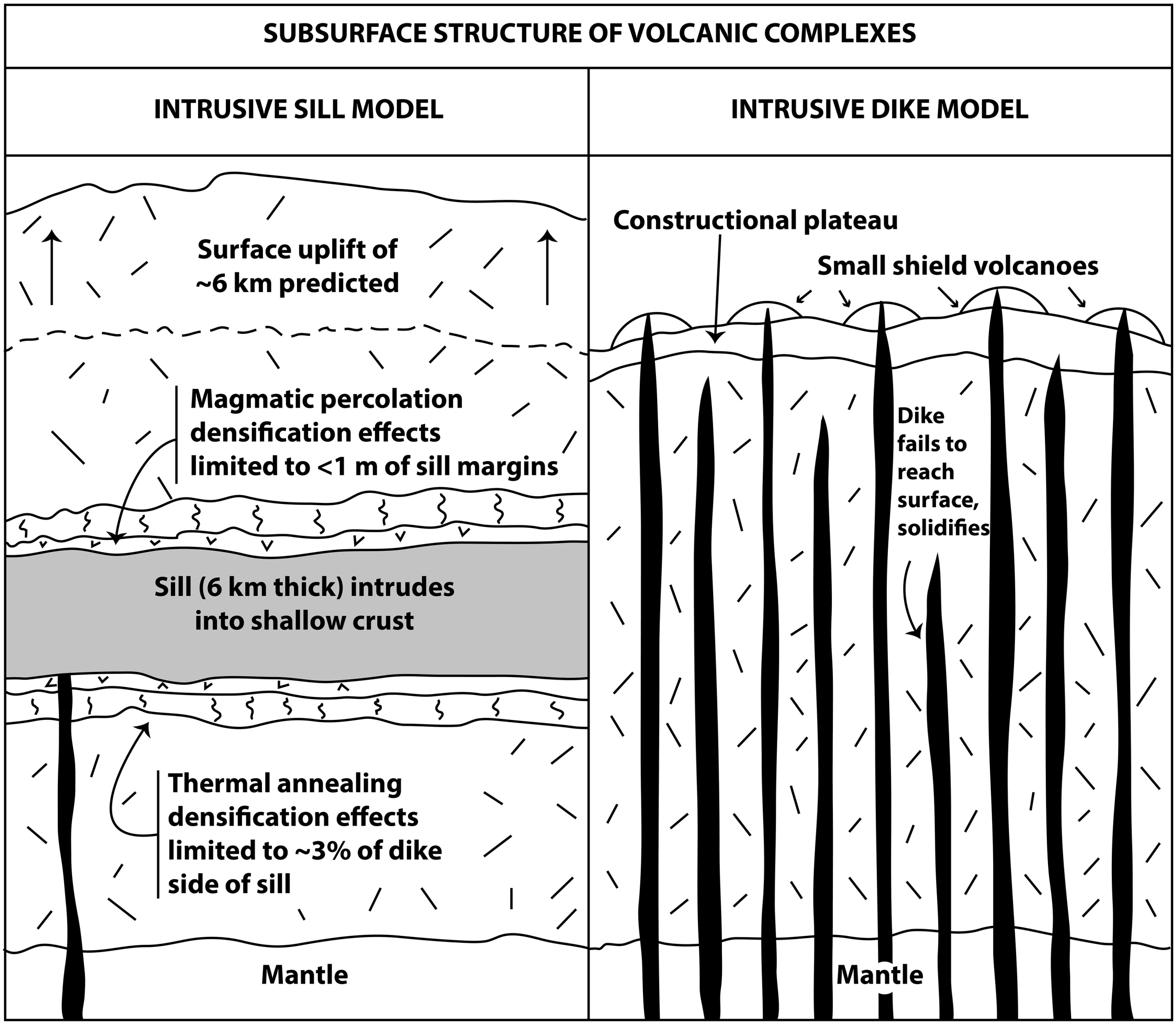

Figure 5
5391
04/08 /19

Table 1. Magma travel distance Z_t while flowing turbulently, subsequent travel distance Z_l after motion becomes laminar, and maximum total penetration distance Z_m for magma intruded into open fractures of width W.

W	Z_t/m	Z_l/m	Z_m/m
1 cm	-	0.01	0.01
3 cm	-	0.78	0.78
5 cm	-	6	6
7.5 cm	4	21	25
10 cm	12	42	54
15 cm	32	117	149
20 cm	57	235	292
25 cm	86	420	506
30 cm	118	652	770
50 cm	267	2,300	2,567
1 m	750	11,000	11,750